

Stereodynamic control of overlapping resonances in cold molecular collisions

Masato Morita,¹ Qian Yao,² Changjian Xie,^{2,3} Hua Guo,² and Naduvalath Balakrishnan¹

¹*Department of Chemistry and Biochemistry, University of Nevada, Las Vegas, Nevada 89154, USA*

²*Department of Chemistry and Chemical Biology,*

University of New Mexico, Albuquerque, New Mexico 87131, USA

³*Institute of Modern Physics, Shaanxi Key Laboratory for Theoretical Physics Frontiers, Northwest University, Xian, Shaanxi 710127, China*

(Dated: March 2, 2022)

Stereodynamic control of resonant molecular collisions has emerged as a new frontier in cold molecule research. Recent experimental studies have focused on weakly interacting molecular systems such as HD collisions with H₂, D₂ and He. We report here the possibility of such control in strongly interacting systems taking rotational relaxation in cold collisions of HCl and H₂. Using explicit quantum scattering calculations in full six dimensions it is shown that robust control of the collision dynamics is possible even when multiple (overlapping) shape-resonances coexist in a narrow energy range, indicating that cold stereochemistry offers great promise for many molecules beyond simple systems. We demonstrate a striking case where two prominent peaks in overlapping resonances are switched-off simultaneously by suitable alignment of the HCl molecule.

Recent progress in cooling and trapping molecules below 1 Kelvin has led to new insights into chemical dynamics, quantum information processing, quantum simulation, and the test of fundamental physics beyond the standard model [1–10]. In particular, the ability to prepare molecules in selected motional, internal and orientational quantum states has allowed interrogation of molecular events with unprecedented precision. The suppression of higher-order angular momentum partial waves in cold collisions provides an ideal platform to explore state-to-state chemistry with partial wave resolution.

A series of papers by Perreault *et al.* [11–13] laid groundwork for cold stereodynamics [14–17] by combining cold molecular beam technology and coherent optical control of molecular states. They demonstrated stereodynamic control of rotational quenching of vibrationally excited HD ($v = 1, j = 2$) in cold collisions with H₂, D₂ and He [11–13] in a single molecular beam. The initial molecular state of HD, including the bond axis alignment, was prepared by Stark-induced adiabatic Raman passage (SARP) [18, 19]. The quenching rate and angular distribution were found to vary significantly depending on whether the HD bond axis is preferentially aligned horizontal (H-SARP) or vertical (V-SARP) to the initial relative velocity vector between the collision partners, providing conclusive evidence of strong stereodynamic effect in HD+H₂/D₂ collisions near 1 Kelvin.

While the collision energies involved in the experiment are narrow (< 5 K) and only a limited number of partial waves ($\sim l < 5$) is involved, the experiments do not provide energy or partial wave resolution directly. In a subsequent theoretical study Croft *et al.* [20] attributed key feature of the angular distribution of the rotationally de-excited HD to an incoming d -wave ($l = 2$) shape resonance centered at about 1 K. The role of isolated (shape) resonances in controlling quenching rate and overall angular distribution of the products was further

explored in theoretical studies of HD+H₂ [21, 22] and in recent experiments on HD+He [13].

As a straightforward extension of H-SARP and V-SARP, it is possible to consider a continuous control of the preferential alignment of the HD bond axis to the initial relative velocity vector by varying the polarization direction of the SARP laser with respect to molecular beam axis. This allows explicit control of the scattering resonance as demonstrated by theoretical studies of Croft and Balakrishnan [21] and Jambrina *et al* [22] for HD+H₂. We note that, experimental SARP technology has the capability to achieve such flexible control of molecular states [13, 19] and it is applicable to a broad class of molecules including those with no permanent electric dipole moment [23, 24].

These advances now allow controlled studies of molecular collisions and chemical reactions using fully tailored molecular initial rovibrational states (v, j, m) and their coherent superpositions, where m is the projection of j onto a quantization axis. Such investigations of systems beyond HD+H₂, HD+D₂ and HD+He are crucial to unveil whether the stereodynamic control is possible for broader classes of molecules with stronger intermolecular interactions. In particular, stereodynamic effect in the presence of multiple (overlapping) resonances in cold collisions is an open question that remains to be addressed.

In this Letter, we examine this question by taking rotational quenching of HCl by collisions with H₂ in the sub-Kelvin regime based on full-dimensional quantum scattering calculations on a recently reported *ab initio* potential energy surface (PES) [25]. This system is of current experimental interest in Zare’s group (private communication). In comparison with HD, the HCl molecule is strongly dipolar (dipole moment ~ 1.08 D) and is amenable to high optical controllability of its internal states. The HCl+H₂ interaction potential is deeper and more anisotropic [25] leading to strong

coupling between the different rovibrational channels at short range. The small rotational constant of HCl (a factor of 5 smaller than HD) also contributes to the increased density of states and more complex collision dynamics for the HCl+H₂ system.

Details of the *ab initio* PES for HCl+H₂ and its analytical representation are reported previously [25]. Briefly, the PES consists of a short-range part fit to high-level *ab initio* data and a long-range part giving an accurate description of the electrostatic and dispersion interactions. The depth of the interaction potential well is ~ 216 cm⁻¹, significantly deeper than that between two H₂ molecules (~ 35 cm⁻¹). The time-independent Schrödinger equation for the molecular scattering is numerically solved using the close-coupling method as implemented in the TwoBC code [26, 27]. More details of the computational approach can be found in previous publications [20, 21, 25] and we limit our discussions to key notations and essential formulas.

The state-to-state differential cross section (DCS) for isotropic collisions (no alignment) in the helicity representation is given by [28]

$$\frac{d\sigma_{\alpha \rightarrow \alpha'}}{d\Omega} = \frac{1}{(2j_1 + 1)(2j_2 + 1)} \sum_{k_1, k_2, k'_1, k'_2} |q_{\alpha, k_1, k_2 \rightarrow \alpha', k'_1, k'_2}|^2, \quad (1)$$

where $\alpha \equiv v_1 j_1 v_2 j_2$ and $\alpha' \equiv v'_1 j'_1 v'_2 j'_2$ refer to the initial and final combined molecular rovibrational states, respectively, $d\Omega$ is the infinitesimal solid angle, the subscript 1 refers to HCl and 2 to H₂. The quantum number k/k' is the projection of the initial/final molecular rotation angular momentum j/j' onto the BF z-axis. The θ dependence in the scattering amplitude is given as [20, 21, 28]

$$\begin{aligned} q_{\alpha, k_1, k_2 \rightarrow \alpha', k'_1, k'_2} &= \frac{1}{2k_\alpha} \sum_J (2J + 1) \sum_{j_{12}, j'_{12}, l, l'} i^{l-l'+1} T_{\alpha j_{12} l, \alpha' j'_{12} l'}^J(E) d_{k_{12}, k'_{12}}^J(\theta) \\ &\times \langle j'_{12} k'_{12} J - k'_{12} | l' 0 \rangle \langle j_{12} k_{12} J - k_{12} | l 0 \rangle \\ &\times \langle j'_1 k'_1 j'_2 k'_2 | j'_{12} k'_{12} \rangle \langle j_1 k_1 j_2 k_2 | j_{12} k_{12} \rangle, \end{aligned} \quad (2)$$

where k_α is the wave number for the incident channel, J is the quantum number of the total angular momentum of the collision complex defined as $\mathbf{J} = \mathbf{j}_{12} + \mathbf{l}$ with the combined rotational angular momentum \mathbf{j}_{12} of the two molecules given by $\mathbf{j}_{12} = \mathbf{j}_1 + \mathbf{j}_2$ and the relative orbital angular momentum \mathbf{l} between the collision partners. The T -matrix is given in terms of the S -matrix as $T = 1 - S$, E is the total energy, and $d_{k_{12}, k'_{12}}^J(\theta)$ is the Wigner's reduced rotation matrix, and the bracket $\langle | \rangle$ denotes a Clebsch-Gordan coefficient. We note that k_{12} and k'_{12} in Eq. (2) mean $k_1 + k_2$ and $k'_1 + k'_2$, respectively.

By taking the integral of the DCS in Eq. (1) over θ and ϕ one obtains the state-to-state integral cross section

(ICS) as [25, 27, 28]

$$\begin{aligned} \sigma_{\alpha \rightarrow \alpha'}(E) &= \frac{\pi}{(2j_1 + 1)(2j_2 + 1)k_\alpha^2} \\ &\times \sum_{j_{12}, j'_{12}, l, l'} (2J + 1) |\delta_{\alpha j_{12} l, \alpha' j'_{12} l'} - S_{\alpha j_{12} l, \alpha' j'_{12} l'}^J(E)|^2. \end{aligned} \quad (3)$$

Eqs. (1) and (3) include averaging over all possible initial orientations of the molecular rotational states specified by the projections k_1 and k_2 . Our primary goal is to explore the effect of aligning the HCl bond axis relative to the initial relative velocity vector for the collision (BF z-axis), as explored in previous studies of HD [11, 12, 21, 22]. In this scheme the initial rotational state of HCl is prepared as $|j_1, \tilde{m}_1 = 0\rangle$ by the laboratory fixed SARP laser where \tilde{m}_1 is the projection of j_1 onto the linear polarization direction of the SARP laser. The prepared state $|j_1, \tilde{m}_1 = 0\rangle$ can be expressed as a coherent superposition of a set of states $|j_1, k_1\rangle$ specified by the projection j_1 onto the BF z-axis as [21]

$$|j_1, \tilde{m}_1 = 0\rangle = \sum_{k_1 = -j_1}^{j_1} d_{\tilde{m}_1 = 0, k_1}^{j_1}(\beta) |j_1, k_1\rangle, \quad (4)$$

where β is the angle between the aligned HCl bond axis and the initial relative velocity vector for the collision.

For rotational quenching of aligned HCl by cold collision with *para*-H₂ ($j_2 = 0, k_2 = 0$), the state-to-state DCS with respect to the scattering angle θ is given by [21]

$$\left(\frac{d\sigma}{d\theta}\right)_\beta = 2\pi \sin\theta \sum_{k_1 = -j_1}^{j_1} \sum_{k'_1 = -j'_1}^{j'_1} |d_{0, k_1}^{j_1}(\beta)|^2 |q_{\alpha, k_1, 0 \rightarrow \alpha', k'_1, 0}|^2 \quad (5)$$

where it is assumed that, like in previous experiments [11–13], the rotationally de-excited HCl molecules in a specific rotational state (j'_1) are detected with no resolution of their k'_1 or azimuthal angle ϕ . The overall effect of the alignment of the HCl molecules is captured in the weight factor $|d_{0, k_1}^{j_1}(\beta)|^2$ for each $|q|^2$ term associated with an initial k_1 . The behavior of $|d_{0, k_1}^{j_1}(\beta)|^2$ as a function of β for $j_1 = 2$ is displayed in Ref. [21] (see also Fig. S1 in SM [29]).

First we discuss rotational quenching of HCl ($v_1 = 1, j_1 = 2$) \rightarrow ($v'_1 = 1, j'_1 = 0$) by collisions with *para*-H₂ ($j_2 = 0, k_2 = 0$), namely $\Delta j_1 = -2$. The ICS for isotropic collisions is shown by the dashed curve in Fig. 1. Contributions from different incoming partial waves $l = 0$ to $l = 3$ are also shown. It is seen that a pronounced peak at about $E_C = 0.3$ cm⁻¹ has the main contribution (77 %) from an incoming *p*-wave ($l = 1$) and a smaller contribution from an incoming *f*-wave ($l = 3$). The quasi-bound states due to closed channels are inaccessible at these collision energies (see Fig. S2 in SM [29]), thus the observed resonance is a *p*-wave shape resonance. We

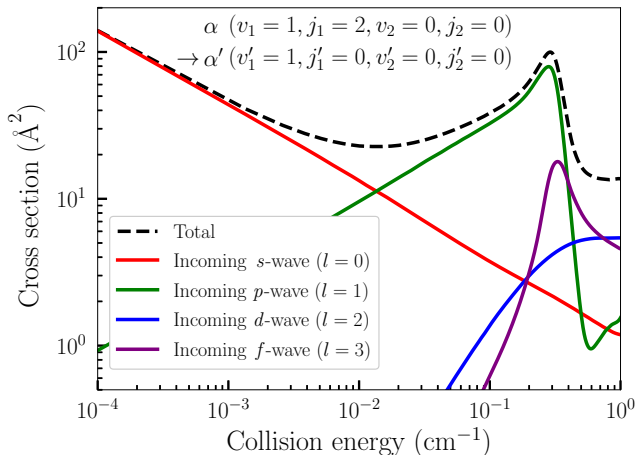


FIG. 1. Integral cross section for the rotational quenching of HCl ($v_1 = 1, j_1 = 2 \rightarrow v_1' = 1, j_1' = 0$) due to collisions with *para*-H₂ ($v_2 = 0, j_2 = 0$) for the isotropic case (no alignment). The dashed black curve shows the total cross section and the solid curves display the partial wave contributions.

note that a *p*-wave shape resonance was not observed for HD+*para*-H₂ collisions [20–22], indicating that cold HCl+H₂ collisions exhibit markedly different features compared to HD+H₂. Indeed, the adiabatic potential energy curves for HCl+H₂ are much more complicated [29] than those of HD+H₂ [20].

We now discuss how to control this resonance by the preparation of initial alignment of the HCl bond axis. The ICS in the resonance region with and without initial alignment of HCl is shown in Fig. 2 (a) using linear axis scale. The dashed curve (isotropic) is identical to the dashed curve (Total) in Fig. 1. Other solid curves correspond to different alignment angles of the HCl bond axis with respect to the initial relative velocity vector for the collision, obtained by integrating the corresponding DCS over θ from 0 to π in Eq. (5). The cross section varies almost monotonically by a factor of 3 as β increases from 0° to 90°, indicating the feasibility of robust control of quenching rate by changing the angle of alignment.

As shown in Eq. (5), the DCS and the resultant ICS are given as the sum of terms specified by the different projection component k_1 of j_1 . Therefore, the observed trend of the ICS in terms of β can be effectively analyzed by examining the ICS with initially oriented HCl specified by a projection k_1 (Fig. 2 (b)). Note that the result for $k_1 = 0$ is the same as $\beta = 0$ in Fig. 2 (a). The cross sections for other values of k_1 are relatively suppressed in the resonance region. In particular, a shallow dip is observed for $|k_1| = 2$.

The above findings indicate that the sensitive dependence of the dynamics in the resonance region to the initial orientation (specified by k_1) of HCl can cause

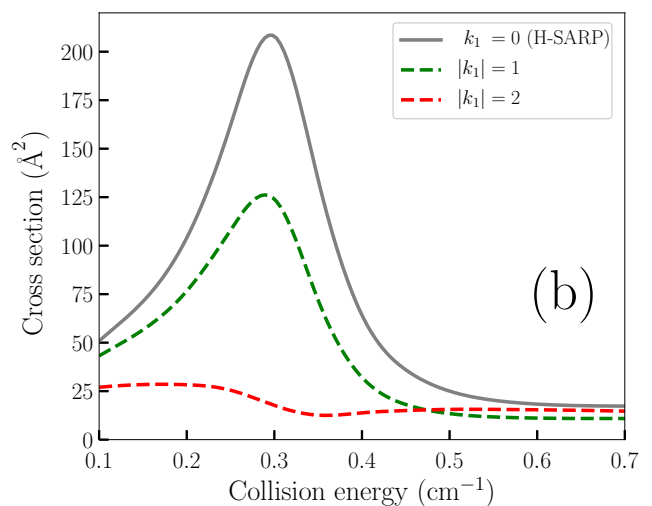
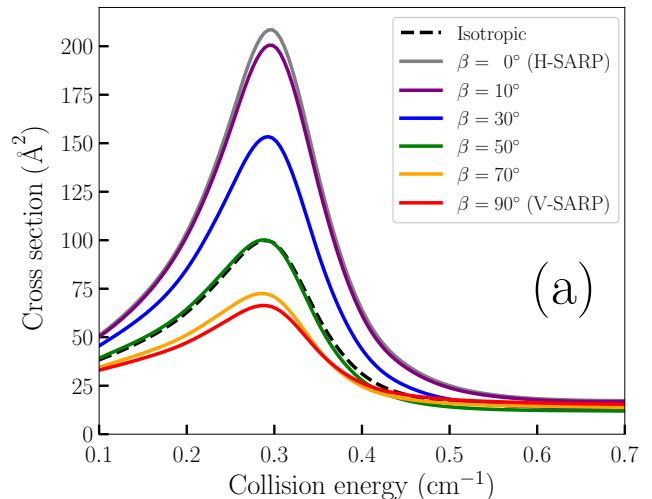


FIG. 2. Integral cross section for $\Delta j = -2$ transition in HCl: (a) for different alignments of HCl bond axis against the initial relative velocity vector for the collision. (b) for different orientations specified by the projection k_1 of the initial rotational state of HCl ($j_1 = 2$). The result for $k_1 = 0$ is identical to that of $\beta = 0^\circ$ in (a).

dramatic change in collision outcome. Compared to $|k_1| = 2$, the ICS for $k_1 = 0$ is about 12-fold larger at the peak of the resonance ($E_C = 0.3 \text{ cm}^{-1}$). Since the projections of the final rotational states are $k_1' = 0$ and $k_2' = k_2 = 0$ due to $j_1' = 0$ and $j_2' = j_2 = 0$, collisions with $k_1 = 0$ conserve helicity as $k_1 + k_2 = k_1' + k_2' = 0$ and the resonance enhancement can be attributed to a helicity conserving transition. It is worth pointing out that results in Fig. 2 (a) do not reflect the full potential of stereodynamic control. If it is possible to specifically prepare an initial HCl rotational state with $k_1 = 2$ or $k_1 = -2$, or their linear combination, the resonance can be completely switched off. Recent advances in SARP

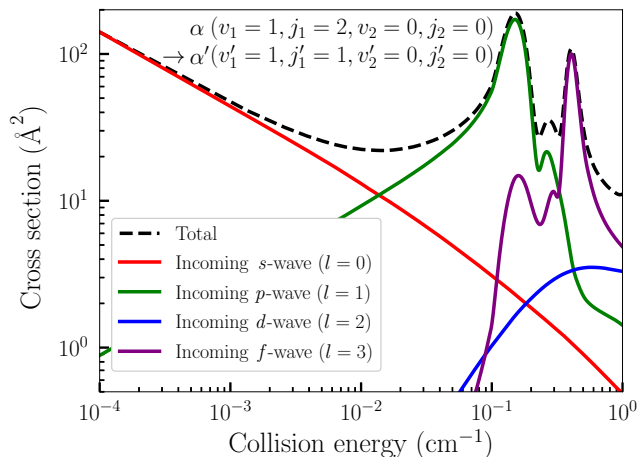


FIG. 3. The same as in Figure 1 but for $\Delta j = -1$ transition.

techniques have made progress in this direction [13, 19]. Indeed, preparation of a phase-locked superposition of $k_1 = \pm 1$ states, $\sqrt{1/2}(|j_1 = 2, k_1 = 1 \rangle + |j_1 = 2, k_1 = -1 \rangle)$, termed X-SARP, was demonstrated for HD [13], expanding the range of control achievable using SARP techniques. The range of control expands into the non-resonant region for the DCS as shown in the Supplemental Material [29].

Next we examine $\Delta j_1 = -1$ transition in HCl, i.e., $(v_1 = 1, j_1 = 2) \rightarrow (v'_1 = 1, j'_1 = 1)$. Figure 3 presents the total and partial wave resolved ICSs for this process for the isotropic case. The crucial difference here in comparison with Fig. 1 is the enhanced incoming f -wave contribution at around 0.4 cm^{-1} in addition to a strong p -wave resonance at about 0.15 cm^{-1} leading to two prominent peaks. While the two resonances appear as distinct peaks in close proximity we note that the p -wave peak has a small contribution from the f -wave resonance illustrating the complex nature of the dynamics and partial overlap of these resonances. This brings up an important question that has not been addressed before: can stereodynamic control be effective for such overlapping resonances associated with multiple partial waves? In previous studies of HD+H₂, HD+D₂ and HD+He, the stereodynamic effect was attributed to the characteristics of a specific isolated shape resonance. However, such simplicity is not necessarily expected for vast majority of systems due to the higher density of states caused by the stronger interaction and/or heavier mass.

As shown in Fig. 4 (a) the angle (β) between the aligned HCl bond axis and the initial relative velocity vector for the collision has a strong effect on the magnitude of both resonances. However, some notable differences are also visible compared to the $\Delta j_1 = -2$ transition (Fig. 2 (a)). In Fig. 4 (a), the f -wave shape

resonance peak increases in intensity with increasing β from 0° to 90° , just the opposite of the trend observed for the peak in $\Delta j_1 = -2$ transition. The p -wave peak at lower energy increases in intensity with increasing β but it saturates at around 50° before eventually decreasing with increasing β (from 70° to 90°). Nevertheless, both resonances exhibit considerable range of control by the alignment preparation. In particular, with small value of β ($< 10^\circ$), both peaks are essentially switched off.

To gain more insights into the two resonances Fig. 4 (b) presents ICS with different initial HCl orientations. The cross section for $k_1 = 0$ is the smallest near the resonance peaks and exhibits a small bump near 0.3 cm^{-1} , the region in between the two resonances. On the other hand, we observe two intense peaks with $|k_1| = 1$ and 2 , revealing the origin of the overlapping resonances. Unlike the $\Delta j_1 = -2$ results shown in Fig. 2 (b), $|k_1| = 2$ gives the largest cross sections while it does not conserve the helicity ($k_1 + k_2 \neq k'_1 + k'_2$). It means that the resonances for $\Delta j_1 = -2$ and $\Delta j_2 = -1$ transitions do not share the same mechanism. While the interaction potential does not directly contribute to change in the helicity $k_1 + k_2$, the centrifugal term can induce it (Coriolis coupling), and the combined effect of these terms determines the resulting resonance profile. Recent studies of molecular reaction and spin-relaxation in the cold energy regime have also pointed out that approximate calculations assuming the conservation of helicity tend to fail in resonance regions [30, 31].

In summary, we have demonstrated flexible and robust control of resonant rotational quenching of HCl in cold collisions with H₂ at the level of integral cross sections by preparing HCl in an aligned or oriented state in the $v = 1$ vibrational level. The most striking result of our study is that even multiple peaks due to resonances associated with disparate partial waves can be controlled, indicating that stereodynamic control is not limited to simple systems with isolated resonances. Our results also reveal the importance of helicity-nonconserving transitions in stereodynamic control of resonant molecular collisions. The analysis based on the initial orientations of HCl rotational state demonstrates the enormous potential controllability in cold molecular collisions, which is tractable with current experimental techniques.

We are grateful to James Croft and Nandini Mukherjee for stimulating discussions. This work is supported in part by NSF grant No. PHY-1806334 (N.B.) and ARO MURI grant No. W911NF-19-1-0283 (N.B. and H.G.).

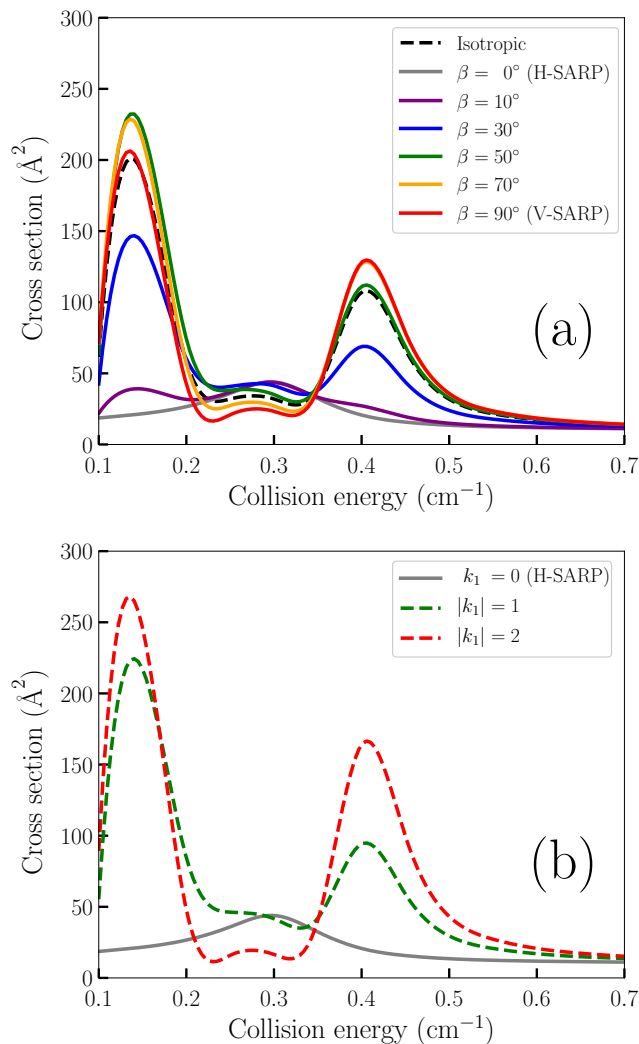


FIG. 4. The same as in Figure 2 but for $\Delta j = -1$ transition.

[1] K. M. Jones, E. Tiesinga, P. D. Lett, and P. S. Julienne, *Rev. Mod. Phys.* **78**, 483 (2006).
 [2] R. V. Krems, *Phys. Chem. Chem. Phys.* **10**, 4079 (2008).
 [3] L. D. Carr, D. DeMille, R. V. Krems, and J. Ye, *New J. Phys.* **11**, 055049 (2009).
 [4] C. Naulin and M. Costes, *Int. Rev. Phys. Chem.* **33**, 427 (2014).
 [5] B. K. Stuhl, M. T. Hummon, and J. Ye, *Ann. Rev. Phys. Chem.* **65**, 501 (2014).
 [6] N. Balakrishnan, *J. Chem. Phys.* **145**, 150901 (2016).
 [7] J. L. Bohn, A. M. Rey, and J. Ye, *Science* **357**, 1002 (2017).
 [8] M. S. Safronova, D. Budker, D. DeMille, D. F. J. Kimball, A. Derevianko, and C. W. Clark, *Rev. Mod. Phys.* **90**, 025008 (2018).
 [9] Y. Shagam, A. Klein, W. Skomorowski, R. Yun, V. Averbukh, C. P. Koch, and E. Narevicius, *Nat. Chem.* **7**, 921

(2015).
 [10] Y. Segev, M. Pitzer, M. Karpov, N. Akerman, J. Narevicius, and E. Narevicius, *Nature* **572**, 189 (2019).
 [11] W. E. Perreault, N. Mukherjee, and R. N. Zare, *Science* **358**, 356 (2017).
 [12] W. E. Perreault, N. Mukherjee, and R. N. Zare, *Nat. Chem.* **10**, 561 (2018).
 [13] W. E. Perreault, N. Mukherjee, and R. N. Zare, *J. Chem. Phys.* **150**, 174301 (2019).
 [14] R. N. Zare, *Science* **279**, 1875 (1998).
 [15] A. J. Orr-Ewing, *J. Chem. Soc., Faraday Trans.* **92**, 881 (1996).
 [16] J. Aldegunde, M. P. de Miranda, J. M. Haigh, B. K. Kendrick, V. Sáez-Rábanos, and F. J. Aoiz, *J. Phys. Chem. A* **109**, 6200 (2005).
 [17] F. Wang, K. Liu, and T. P. Rakitzis, *Nat. Chem.* **4**, 636 (2012).
 [18] W. Dong, N. Mukherjee, and R. N. Zare, *J. Chem. Phys.* **139**, 074204 (2013).
 [19] N. Mukherjee, W. Dong, and R. N. Zare, *J. Chem. Phys.* **140**, 074201 (2014).
 [20] J. F. E. Croft, N. Balakrishnan, M. Huang, and H. Guo, *Phys. Rev. Lett.* **121**, 113401 (2018).
 [21] J. F. E. Croft and N. Balakrishnan, *J. Chem. Phys.* **150**, 164302 (2019).
 [22] P. G. Jambrina, J. F. E. Croft, H. Guo, M. Brouard, N. Balakrishnan, and F. J. Aoiz, *Phys. Rev. Lett.* **123**, 043401 (2019).
 [23] W. Dong, N. Mukherjee, and R. N. Zare, *J. Chem. Phys.* **139**, 074204 (2013).
 [24] W. E. Perreault, N. Mukherjee, and R. N. Zare, *J. Chem. Phys.* **150**, 234201 (2019).
 [25] Q. Yao, M. Morita, C. Xie, N. Balakrishnan, and H. Guo, *J. Phys. Chem. A* **123**, 6578 (2019).
 [26] R. V. Krems, *TwoBC Quantum Scattering Program*, Vancouver: University of British Columbia (2006).
 [27] G. Qummer and N. Balakrishnan, *J. Chem. Phys.* **130**, 114303 (2009).
 [28] J. Schaefer and W. Meyer, *J. Chem. Phys.* **70**, 344 (1979).
 [29] See Supplemental Material at [http://link.***.org/supplemental/XXX/] for squared Wigner's reduced rotational matrix elements, adiabatic and diabatic potential energy curves, differential cross section, and integral cross section for minor transitions associated with vibrational relaxation of HCl.
 [30] G. Qummer and N. Balakrishnan, *J. Chem. Phys.* **128**, 224304 (2008).
 [31] M. Morita and T. V. Tscherebul, *J. Chem. Phys.* **150**, 074110 (2019).

Supplemental Material

Stereodynamic control of overlapping resonances with aligned cold molecules

Masato Morita, Qian Yao, Changjian Xie, Hua Guo and Naduvalath Balakrishnan

S-I. Weighting factor for the aligned HCl

As outlined in the main text, the HCl bond axis is preferentially aligned parallel to the linear polarization direction of the SARP laser (pump and Stokes laser pulses which intersect the laboratory fixed molecular beam) and the rotational state is written as $|j_1, \tilde{m}_1 = 0\rangle$, where \tilde{m}_1 is the projection of j_1 onto an axis parallel to the polarization of the SARP laser. The state can be expressed as a coherent superposition of rotational states $|j_1, k_1\rangle$ ($k_1 = -j_1, -j_1 + 1, \dots, j_1 - 1, j_1$), where k_1 is the projection of j_1 onto the z-axis of the body-fixed coordinate frame which is parallel to the relative velocity vector for the collision. As a function of the angle (β) between the (preferentially aligned) HCl molecular bond axis and the initial relative velocity vector for the collision, the coefficients for the superposition are given by Wigner's reduced rotation matrix as $d_{0,k_1}^{j_1}(\beta)$. The differential cross section as a function of θ is expressed using the squared value $|d_{0,k_1}^{j_1}(\beta)|^2$ as the weighting factor for each $|q|^2$ term associated with k_1 as long as the azimuthal angle (ϕ) dependence of the scattering is averaged over by taking the integral as mentioned in the main text. Since the cross section is given as the sum of positive valued terms, the magnitude of the weighting factor is essential to analyze the cross section. For $j_1 = 2$, the weighting factor $|d_{0,k_1}^2(\beta)|^2$ associated with 5 possible k_1 terms ($k_1 = -2, -1, 0, 1, 2$) is shown below (Fig. S1). An essentially identical figure is shown in Ref. [21] for the study of HD+H₂. For example, $\beta = 0^\circ$ corresponds to H-SARP, and the term associated with $k_1 = 0$ has a weighting factor of 1.0 because the HCl molecular bond axis is preferentially aligned parallel to the initial relative velocity vector for the collision. For $\beta = 90^\circ$ corresponding to the V-SARP preparation, the terms associated with $k_1 = \pm 1$ make no contribution.

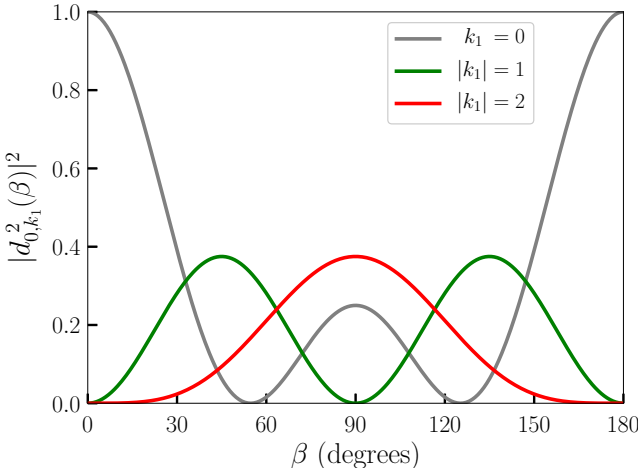


FIG. S1. Weighting factor $|d_{0,k_1}^2(\beta)|^2$ for the aligned HCl ($j_1 = 2, \tilde{m}_1 = 0$) as a function of β . The quantum number k_1 is the projection of j_1 onto the initial relative velocity vector between the collision partners. The angle between the aligned HCl molecular bond axis and the initial relative velocity vector is denoted by β .

S-II. Adiabatic and diabatic potential energy curves

The collision dynamics of HCl+H₂ is more complex compared with previously studied HD+H₂ [20] due to the larger anisotropy and deeper well depth of the HCl+H₂ PES and the smaller rotational constant of HCl. These characteristics give rise to strong interchannel coupling and high density of states/resonances.

Quantum scattering calculations are performed to obtain the scattering S -matrix using the close-coupling (CC) method on a full six-dimensional (6D) *ab initio* PES obtained in our recent work [25]. An analytical fit of the PES using the permutation invariant polynomial neural network (PIP-NN) method was performed based on the grid points calculated with CCSD(T)-F12b/aug-cc-pVQZ (AVQZ). The CC equations for the HCl+H₂ collision complex obtained using the total angular momentum basis set $|JM(lj_{12}(j_1j_2))\rangle$ for the angular variables in a space-fixed (SF) coordinate frame are numerically solved by the log-derivative propagation method using the TwoBC code.

Here, we show the adiabatic and diabatic potential energy curves for HCl+H₂ and provide further insights into the strong coupling at short-range during the collision. The diabatic potential energy curves with the basis set

$$r_1^{-1}\phi_{v_1}^{j_1}(r_1)r_2^{-1}\chi_{v_2}^{j_2}(r_2)|JM(lj_{12}(j_1j_2))\rangle, \quad (\text{S1})$$

where $\phi_{v_1}^{j_1}$ and $\chi_{v_2}^{j_2}$ are the radial part of the eigenfunctions of rovibrational states of HCl and H₂, are defined as the diagonal elements of the effective potential $W(R)$ in Eq. (S2) below. On the other hand, the adiabatic potential energy curves are given as the eigenvalues obtained by diagonalizing the $W(R)$ matrix at each value of the parameter R , thus, in principle, the adiabatic potential energy curves are independent of basis sets. The matrix element in $W(R)$ in the basis set (Eq. (S1)) is written as

$$\begin{aligned} W_{\alpha j_{12}l, \alpha' j'_{12}l'}^{J, \epsilon_I}(R) &= \frac{l(l+1)\hbar^2}{2\mu R^2} \delta_{\alpha j_{12}l, \alpha' j'_{12}l'} + V_{\alpha j_{12}l, \alpha' j'_{12}l'}^{J, \epsilon_I}(R) \\ &= [E_\alpha^0 + \frac{l(l+1)\hbar^2}{2\mu R^2}] \delta_{\alpha j_{12}l, \alpha' j'_{12}l'} + U_{\text{int}}^{J, \epsilon_I}_{\alpha j_{12}l, \alpha' j'_{12}l'}(R), \end{aligned} \quad (\text{S2})$$

where $\alpha \equiv v_1j_1v_2j_2$ refers to the combined molecular state, ϵ_I is the inversion parity defined as $(-1)^{l+j_1+j_2}$, μ is the reduced mass for the molecular collision, $V(R)$ is the potential energy of the tetra-atomic system, E_α^0 denote the channel energies for the separated molecules whose quantum states are specified by α and $U_{\text{int}}(R)$ is the interaction potential between HCl and H₂. Here, we shows the adiabatic and diabatic potential energy curves obtained with $J = 3$ and $\epsilon_I = -1$ because the incoming p -wave ($l = 1$), which generates the shape resonance discussed in the main text, is included for the initial state $\alpha \equiv (1, 2, 0, 0)$ in this study.

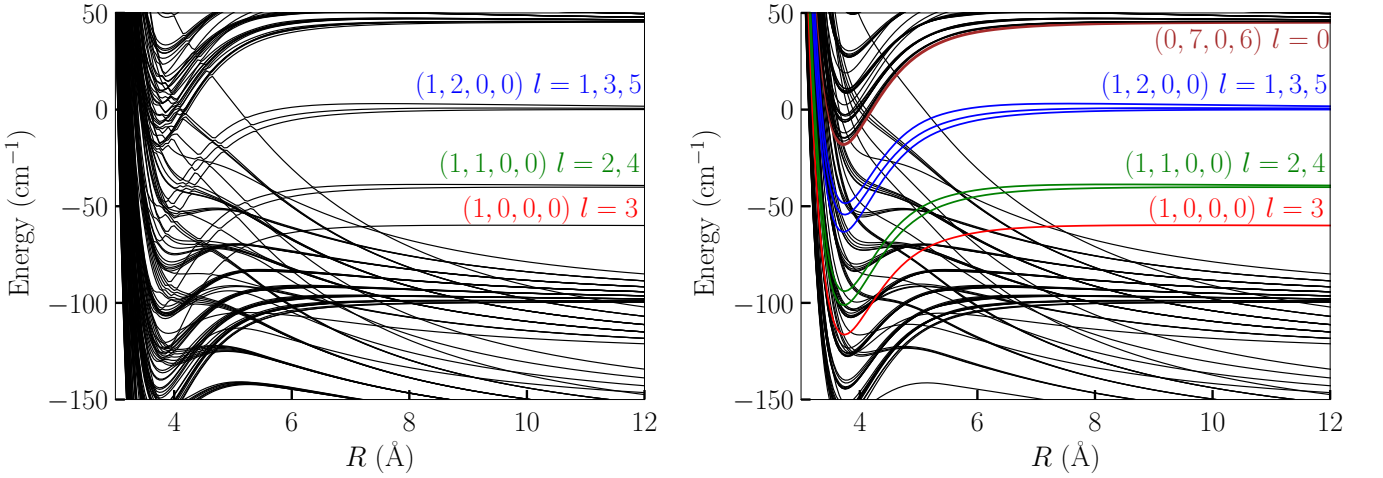


FIG. S2. Adiabatic (left panel) and diabatic (right panel) potential energy curves for HCl+H₂ with the total angular momentum basis set ($J = 3$ and $\epsilon_I = -1$). R is the distance between the centers of mass of HCl and H₂. Some relevant diabatic states are highlighted with colors and their combined rovibrational states α and associated orbital angular momenta are specified as $\alpha = (v_1, j_1, v_2, j_2)$ and l , respectively. The zero energy of the vertical axis is the dissociation limit between HCl ($v_1 = 1, j_1 = 2$) and H₂ ($v_2 = 0, j_2 = 0$) which is the initial scattering state in this study.

The adiabatic potential energy curves in the left panel of Fig. S2 exhibit multiple avoided crossings, in particular at shorter R range, which are significantly different from the HD+H₂ case studied in previously [20]. For HD+H₂, the relevant adiabatic potential energy curves did not feature avoided crossings, leading to smooth well-separated curves in the entire range of R . Consequently, the collision dynamics of HCl+H₂ is much complicated compared to that

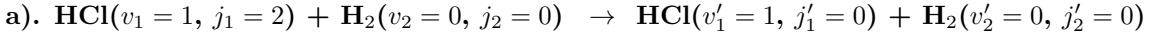
of HD+H₂. While the crossings are not necessarily strongly avoided, we observe several series of crossings through a wide R range due to the repulsive curves associated with higher partial waves for the highly rotationally excited molecules in their vibrational ground states.

While the diabatic potential energy curves (right panel) do not contain the information about the strength of coupling with other channels, they are more easier to interpret. Near the potential minimum in R of the blues curves corresponding to the initial rovibrational state $\alpha \equiv (1, 2, 0, 0)$, we observe some black curves and a brown curve associated with the closed channels such as $\alpha \equiv (0, 7, 0, 6)$ come down in energy below the dissociation limit of initial state (blue curves). The bound states in those closed channels may couple with incoming partial waves in the incident channel and lead to Feshbach resonances. A bound state calculation of the s -wave component of $\alpha \equiv (0, 7, 0, 6)$ channel (brown curve) yields the lowest bound state energy to be about 13.8 cm^{-1} relative to the incident channel. This rules out a Feshbach resonance in the cold energy regime. Therefore, the resonances in the cold energy regime described in this work are shape resonances caused by the centrifugal barriers for the incoming partial waves.

S-III. Differential cross section

In the main text we discussed the ICS for rotational quenching of HCl ($v_1 = 1, j_1 = 2$) and demonstrated the significant stereodynamic effect in the resonance region. The differential cross section (DCS) is generally more sensitive to the preparation of alignment and orientation of initial molecules if examined under a fine resolution of the scattering angle θ . In the following, we explore stereodynamic effect on DCS for the rotational quenching processes explored in the main text.

In previous experiments for HD collisions with H₂, D₂ and He [11–13], the angular θ distribution of the rotationally de-excited HD in a specific rotational state of j'_1 was probed by combining multi-photon ionization and time-of-flight spectrum. Since the azimuthal angle (ϕ) dependence of the de-excited HD (j'_1) was not observed in the experiments, the ϕ dependence is averaged over by taking the integral from 0 to 2π assuming that there is no detection sensitivity or filtering about ϕ in the experiments. To simplify the discussion, DCS is calculated with oriented initial HCl rotational state specified by the value of k_1 (Fig. S3). Like ICS, the DCS with a general initial HCl alignment by SARP laser can be estimated from the β -dependence of the weighting factor in Fig. S1.



The DCS with the initial state of HCl ($v_1 = 1, j_1 = 2, k_1$) at a collision energy of $E_C = 10^{-4} \text{ cm}^{-1}$ is shown in the left panel of Fig. S3. The resulting angular distributions exhibit symmetric behavior about $\theta = \pi/2$ and clear periodic oscillations with respect to θ , indicating that the only the incoming s -wave ($l = 0$) and the associated outgoing partial wave contribute substantially at such a low energy. The ICS does not have a strong k_1 dependence at off-resonant energies, low energies in particular. Thus it is difficult see the steric effect by observing the ICS alone. The k_1 dependence of the angular distributions provides a much more sensitive probe of stereodynamics.

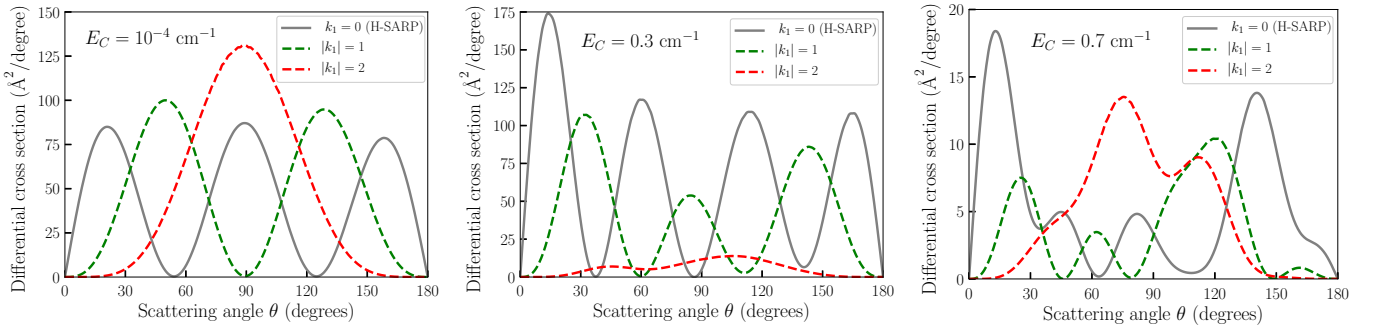
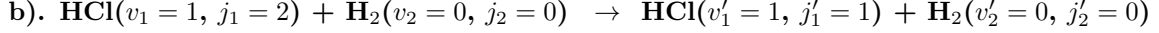


FIG. S3. Differential cross section for the rotational quenching of HCl ($v_1 = 1, j_1 = 2 \rightarrow v'_1 = 1, j'_1 = 0$) due to the collision with *para*-H₂ ($v_2 = 0, j_2 = 0$). Initial rotational state of HCl has a specific value of the projection quantum number k_1 . Collision energies are 10^{-4} cm^{-1} (left panel), 0.3 cm^{-1} (middle panel) and 0.7 cm^{-1} (right panel).

At the peak of the ICS ($E_C = 0.3 \text{ cm}^{-1}$) due to the incoming p -wave ($l = 1$) shape resonance (middle panel of Fig. S3), the symmetry of the angular distribution is lost, in particular for $|k_1| = 2$ while the periodic oscillations of

the cross sections as a function of θ still remain for $k_1 = 0$ and $|k_1| = 1$. The resonance gives rise to a completely different DCS compared to the off-resonant DCS in the low energy region. Furthermore, as shown in the right panel, even at an energy ($E_C = 0.7 \text{ cm}^{-1}$) not far from the resonance, the DCS changes significantly. At this energy, the DCS with $k_1 = 0$ and $|k_1| = 2$ show markedly different angular distributions, thus it would be possible to observe dramatic steric effect if we can control the initial population between these k_1 components. While DCS provides a much more sensitive prob of steric control, angular distribution would be governed by that given at the peak of the resonance when the peak is isolated and pronounced if we do not have a fine resolution in collision energy.



For the final state $j'_1 = 1$ of the HCl molecule, the initial k_1 dependence of the DCS is shown in Fig. S4 at two energies corresponding to the prominent peaks of the overlapping resonances. The dramatically different angular dependence of the DCS at the two energies indicate that the mechanisms of these resonances are completely different. at the collision energy, where we observe the peak of the ICS due to the incoming f -wave ($l = 3$) resonance, (right panel) shows more oscillatory behavior compared to the incoming p -wave ($l = 1$) resonance case (left panel), indicating higher outgoing partial waves (l') are involved for the incoming f -wave resonance. For both cases, the primary contributions arise from $|k_1| = 1$ and 2, a feature also observed in Fig4. (b) of the main text.

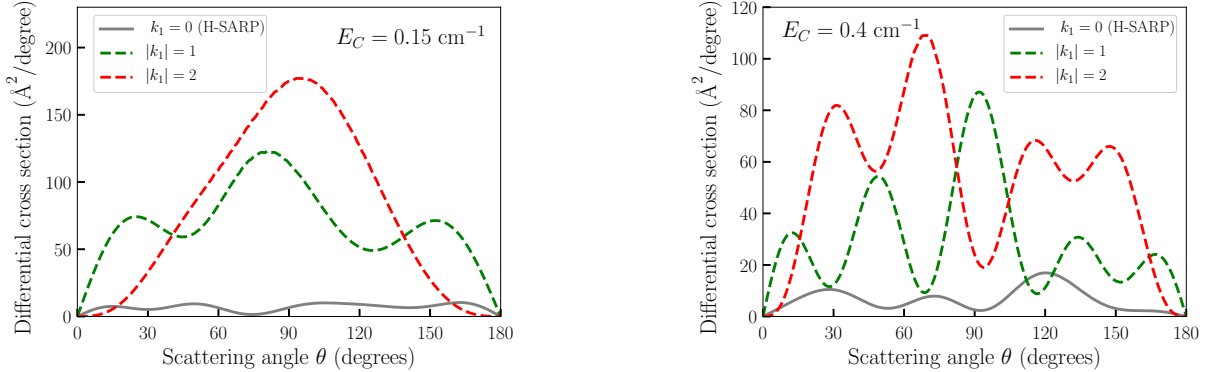


FIG. S4. Differential cross section for the rotational quenching of HCl ($v_1 = 1, j_1 = 2 \rightarrow v'_1 = 1, j'_1 = 1$) due to the collision with *para*-H₂ ($v_2 = 0, j_2 = 0$). Initial rotational state of HCl has a specific value of the projection quantum number k_1 . Collision energies are 0.15 cm^{-1} (left panel) and 0.4 cm^{-1} (right panel).

S-IV. Vibrational relaxations

In the main text, we explored two rotational relaxation processes as in previous studies of HD+H₂ within a vibrational manifold of HCl ($v_1 = 1$). However, if we consider the vibrational relaxation of HCl ($v_1 = 1 \rightarrow v'_1 = 0$), there are many other energetically allowed transitions for HCl+H₂ even in the cold energy regime. As shown below these transitions are much less efficient than pure rotational quenching. Therefore the effects due to these minor vibrational relaxations are negligible in our present study.

There are numerous possible exothermic transition processes from the initial state of HCl ($v_1 = 1, j_1 = 2$) and H₂ ($v_2 = 0, j_2 = 0$). One case is the vibrational relaxation of HCl accompanied by a change of its rotational level. The left panel of Fig. S5 shows the integral cross section (ICS) for these transitions for isotropic (no alignment of molecules) collisions, including the pure vibrational relaxation of HCl ($j_1 = j'_1 = 2$, grey curve). To avoid cluttering in the panel, only transitions to even j'_1 are displayed. The ICS for vibrational quenching of HCl accompanied by rotational excitation of H₂ are displayed in the right panel of Fig. S5. We note that, in this case, only the transitions to even j'_2 are allowed due to the exchange symmetry of H₂.

The presence of the resonance features in the same collision energy regime for these transitions, and also for the rotational quenching studied in the main text, indicate that they are shape resonances associated with specific incoming partial waves and some of them may share the same or similar mechanisms, implying that stereodynamic control of these minor processes would be possible as in the main text. On the other hand, the magnitude and the resonance features are sensitive to the final states, indicating the coupling strength and interference pattern between the multiple resonances strongly depend on the final state.

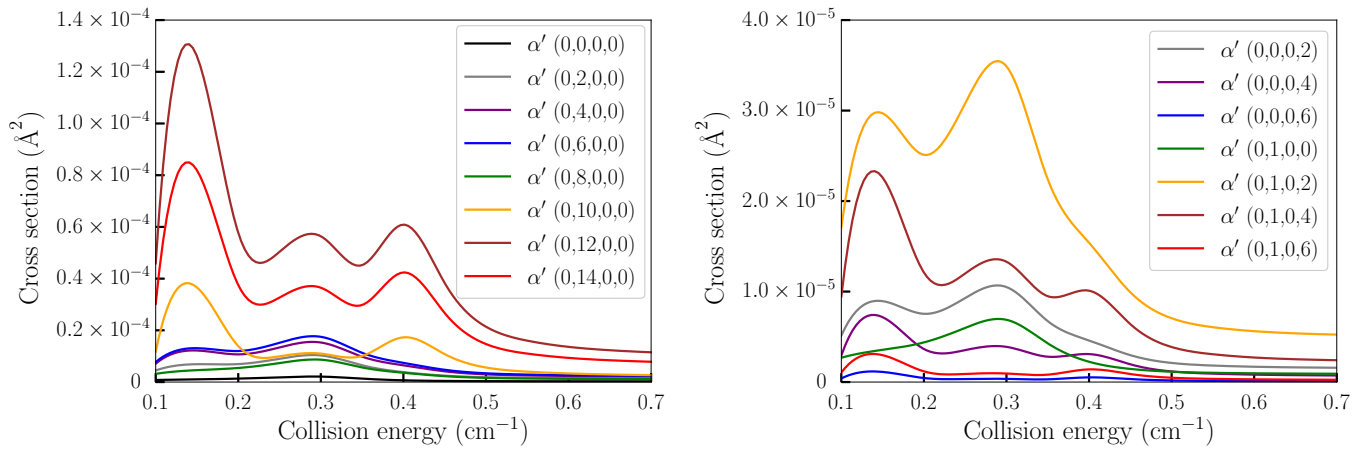


FIG. S5. Integral cross section for the rovibrational transitions of HCl ($v_1 = 1, j_1 = 2$) due to the collision with *para*-H₂ ($v_2 = 0, j_2 = 0$) in the absence of any alignment of molecules. The transitions to the rovibrational states $\alpha' \equiv (v_1' = 0, j_1', v_2' = 0, j_2' = 0)$ (left panel) are shown only for even values of j_1' to avoid cluttering. Rotational transitions of *para*-H₂ ($j_2 = 0 \rightarrow j_2'$) in the transitions to the rovibrational states $\alpha' \equiv (v_1' = 0, j_1' = 0/1, v_2' = 0, j_2')$ (right panel) are allowed only to even values of j_2' due to the exchange symmetry of H₂.